Crystal Structure of the New Layer Silicate RUB-39 and Its Topotactic Condensation to a Microporous Zeolite with Framework Type RRO

Y. X. Wang,[†,‡] H. Gies,*[,†] and J. H. Lin[‡]

Institute of Geology, Mineralogy and Geophysics, Ruhr-University Bochum, D-44780 Bochum, Germany, and College of Chemistry and Molecular Engineering, Peking University, People's Republic of China

Received March 13, 2007. Revised Manuscript Received June 8, 2007

The new synthetic hydrous layer silicate with code RUB-39, $H_2[Si_{18}O_{38}]\cdot 2(C_8H_{20}N)\cdot xH_2O$, was synthesized from hydrothermal solution after 3 weeks at 150 °C and autogenous pressure. The material crystallized as a colorless, fine-grained powder of sub-micrometer crystallite size. The powder diagram was indexed in the monoclinic space group $P2/c$ with $a = 7.33122(5)$ Å, $b = 10.72380(13)$ Å, $c = 17.51354(12)$ Å, and $\beta = 115.69(6)°$. The Rietveld refinement of the crystal structure was refined from laboratory powder X-ray diffraction data based on a structure model derived from the condensation product, zeolite RRO, with final residuals of $R_{wp} = 12.3\%$ and $\chi^2 = 3.1$. The silicate layers of the new hydrous layer silicate are known as subunits of the silicate framework of the natural zeolite mineral heulandite and represent a basic construction principle of silicate framework structures. They are interconnected through strong interlayer hydrogen bonds. The remaining residual void space is filled with the organic template cation and hydrate water. The condensation process has been studied with solid-state NMR and differential thermal analysis/thermogravimetric analysis experiments. A mechanism for the condensation is proposed explaining the almost perfect crystallinity of the three-dimensional framework.

Introduction

Hydrous layer silicates in nature are important minerals originating from weathering processes, occurring as sedimentary minerals, and as products of metamorphic processes. They are also important industrial materials, for example, as raw materials in the porcelain industry, as additives in paints and paper, and as sorbents for cleaning and separation processes.[1] Recently, layer silicates attracted interest as starting materials for topotactic condensation reactions to microporous framework silicates acting as zeolite precursors.[2−5] The concept of using layered precursors for the synthesis of new, three-dimensional framework silicates, in particular microporous zeolites, is of broad general interest, because synthesis of the precursor is carried out at lower temperature, that is, considerably different synthesis conditions, and leads, at the same time, to more economical production processes. In addition, there is also a large variety of natural and synthetic layer silicates with interesting structural features which would lead to microporous framework structures with new types of pore systems if they existed as condensed phases. One research goal of particular interest is, for example, hierarchical pore systems which are difficult to obtain in direct zeolite synthesis.

There are several examples of layered silicate precursors for synthesis of new zeolites which have been studied intensively using diffraction experiments, such as the system Prefer − ferrierite,[6] ITQ-2−MCM-22, ERB-1,[7−9] MCM-65,[11] and CDS-1;[2] however, how the condensation reaction proceeds and why some of the examples lead to highly disordered products and others lead to perfectly ordered crystalline zeolites still remains unclear. Here we report on the structure refinement and the solid-state (SS) NMR investigation of the layered precursor RUB-39, a new hydrous layer silicate, and on the structural changes occurring during the condensation reaction to the zeolite with framework type RRO providing insight into the mechanism of the condensation reaction.

Experimental Section

Synthesis of RUB-39 was carried by using dimethyldipropylammonium hydroxide as the structure directing agent (SDA) and an aqueous dispersion of silica gel in a hydrothermal reactor at

[†] Ruhr-University Bochum.
[‡] Peking University.

(1) Schwieger, W.; Lagaly, G. Alkali silicates and crystalline silicic acids. In *Handbook of Layered Materials*; Scott, S. M., Corrado, K. A., Dutta, P. K., Eds.; Marcel Dekker, Inc.: New York, 2003; Chapter 11, p 541.
(2) Ikeda, T.; Akiyama, Y.; Oumi, Y.; Kawai, A.; Mizukami, F. *Angew. Chem., Int. Ed.* **2004**, *43*, 4892.
(3) Zanardi, S.; Alberti, A.; Cruciani, G.; Corma, A.; Fornés, V.; Brunelli, M. *Angew. Chem., Int. Ed.* **2004**, *43*, 4933.
(4) Marler, B.; Ströter, N.; Gies, H. *Microporous Mesoporous Mater.* **2005**, *83*, 201.
(5) Wang, Y.; Marler, B.; Gies, H.; Müller, U. *Chem. Mater.* **2005**, *17*, 43.
(6) Schreyeck, L.; Caullet, P.; Mougenel, J. C.; Guth, J. L.; Marler, B. *Microporous Mater.* **1996**, *6*, 259.
(7) Leonowicz, M. E.; Lawton, J. A.; Lawton, S. L.; Rubin, M. K. *Science* **1994**, *264*, 1910.
(8) Camblor, M. A., Corma, A.; Dias-Cabanas, M. J.; Baerlocher, C. *J. Phys. Chem. B* **1998**, *102*, 44.
(9) Millini, R.; Perego, G.; Parker, W. O.; Bellussi, G.; Carluccio, L. *Microporous Mater.* **1995**, *4*, 221.
(10) Dorset, D. L.; Kennedy, G. J. *J. Phys. Chem. B* **2004**, *108*, 15216.
(11) Dong, Ch. PowderX. Available at: http://www.ccp14.ac.uk/mirror/mirror.htm.

10.1021/cm0706907 CCC: $37.00
Published on Web 07/21/2007

Table 1. X-ray Data Collection Conditions, Crystallographic Data, and Results of Rietveld Analysis of RUB-39

formula	$H_2[Si_{18}O_{38}]\cdot 2SDA^+$, SDA = $C_8H_{20}N$
crystal system	monoclinic
space group	*P*2/*c* (No. 13)
a, Å	7.33122(5)
b, Å	10.72380(13)
c, Å	17.51354(12)
ss, deg	115.69114(57)
wavelength, Å	1.5406 (Cu Kα_1)
range 2θ (deg)	5−70
step width 2θ (deg)	0.07768
number of points	8335
number of restraints	59
number of structural variables	61
peak profile	Thompson−Cox−Hastings pseudo-Voigt
background correction	linear interpolation of background points
R_F (%)	3.4
R_B (%)	4.6
R_p (%)	13.1
R_{wp} (%)	12.3
χ^2	3.10

150 °C for 3 weeks following the details of the synthesis described elsewhere.[4] In our experience, 150 °C is the upper synthesis temperature for RUB-39. Higher synthesis temperatures yield MFI-type zeolite. For the SS NMR investigation and for thermal studies, the material was recovered from synthesis and dried in an oven at 40 °C. For the powder X-ray diffraction (PXRD) experiment the material was filtered and dried in an oven at 160 °C for 24 h.

SS NMR experiments on ^{1}H and ^{29}Si were carried out on a Bruker ASX-400 using standard Bruker 7 mm probes. For quantitative signal intensities in the ^{29}Si experiments high power decoupling was used with ~10 μs pulses and delay times between pulses of 60 s sufficient for complete recovery of the system. For variable temperature (VT) experiments in the temperature range from room temperature (RT) to 160 °C the proton signals were used to monitor. The samples were allowed to equilibrate at the desired temperature for at least 15 min. To analyze the condensation reaction at temperatures of 250 °C and higher, samples were kept at a temperature externally in an oven for at least 24 h before NMR experiments were carried out with the sample at RT.

Thermal analysis was carried out on a Bähr STA 530 thermal analyzer under constant flow of air using a heating rate of 5°/min.

PXRD experiments were performed on a Siemens D-5000 set up in Debye−Scherrer geometry with monochromatized Cu Kα_1 radiation and a capillary sample holder to prevent preferred orientation. The diffraction data were collected with a Braun position sensitive detector in the degrees 2θ range from 5 to 70 and step width of 0.00778°. Indexing of the powder diagram was carried out with the program Treor-90 implemented in powder-X.[11] The structure was solved from model building and subsequently refined with FullProf.[12] The details of data collection and the results of the structure refinement are summarized in Tables 1−5 and Figure 1, showing the experimental, simulated, and difference X-ray powder diagram of RUB-39.

Results and Discussion

Structure of RUB-39. The results from the indexing of the PXRD pattern of as synthesized RUB-39 clearly showed that the *a*- and *c*-parameters of the monoclinic unit cell were almost the same as those for the condensed framework of zeolite RUB-41, framework type RRO.[13] The *b*-parameter decreased by approximately 2.0 Å after the condensation reaction caused by the elimination of water and the subsequent formation of Si−O−Si bridges during bond formation between adjacent layers (from 10.724 Å to 8.724 Å, cf. Table 1). To confirm the layered structure of RUB-39 and to investigate the composition and the role of intercalated species for the synthesis and during the condensation process, SS magic angle spinning (MAS) NMR experiments were carried out. VT ^{1}H SS MAS NMR spectra were recorded from as-synthesized RUB-39. From the signal at 5.5 ppm it is clear that there is residual water intercalated between the silicate layers evaporating at ~160 °C (Figure 2). The high field proton signals at 3.2, 1.8, and 1.0 ppm can be assigned to the hydrocarbon frame from the tetraalkylammonium SDA which is preserved during the synthesis procedure. The proton signal shifted to the very low field value of 16.7 ppm clearly indicates a strong hydrogen bridge. From the correlation of proton chemical shift values with *d*(O···O) distances[14,15] an estimate of about 2.4 Å can be derived which indicates a very strong hydrogen bond. Similar observations have already been made for hydrogen bridges in other hydrous layer silicates such as RUB-18,[16,17] RUB-15,[18] kanemite,[19] MCM-65,[20] magadiite,[21] and SKS-5.[22] In all cases studied in detail so far, the low field shifted proton bridges two neighboring siloxy groups within the silicate layer and partially compensates for the Coulomb charge of the silicate layer. The intra-layer hydrogen bond thus stabilized the otherwise flexible silicate layer. The remaining charge is compensated by the additional organic or inorganic SDA cation. In all cases studied and mentioned above the strong hydrogen bonds lead to an almost perfect periodic register of neighboring silicate layers with good crystallinity allowing for detailed structure analyses using diffraction experiments. As can be seen from the proton spectra after removing the hydrate water no further structural changes have been observed up to the temperature limit of the VT NMR experiment (Figure 3).

In the ^{29}Si spectrum a typical set of signals for layered silicates has been obtained (Figure 4). At −104.3 ppm the Q^3-signal carrying the silanol group (Si(−O−Si)$_3$OH) and between −108 and −115.4 ppm four Q^4-signals (Si(−OSi)$_4$), typical for framework silicates with integral intensity ratio $Q^3/Q^4 = 2:7$, are observed. The high content of Q^4-Si atoms indicates a high degree of stiffness and rigidity of the silicate layer, comparable to framework silicates. ^{1}H−^{29}Si cross-

(12) (a) Rodriguez-Carvajal, J. *Physica B* **1993**, *193*, 55. (b) FullProf Suite. Available at: http://www.ill.fr/dif/Soft/fp/.

(13) Baerlocher, Ch.; McCusker, L. B. Database of Zeolite Structures. http://www.iza-structure.org/databases/.
(14) Jeffrey, G. A.; Yeon, Y. *Acta Crystallogr.* **1986**, *42*, 410.
(15) Eckert, H.; Yesinowski, J. P.; Silver, L. A.; Stolper, E. M. *J. Phys. Chem.* **1988**, *92*, 2055.
(16) Wolf, I.; Gies, H.; Fyfe, C. A. *J. Phys. Chem. B* **1999**, *103*, 5933.
(17) Borowski, M.; Wolf, I.; Gies, H. *Chem. Mater.* **2002**, *14*, 38.
(18) (a) Oberhagemann, U.; Bayat, P.; Marler, B.; Gies, H.; Rius, J. *Angew. Chem., Int. Ed.* **1996**, *35*, 2869. (b) Gies, H.; Marler, B. To be published.
(19) Apperley, D. C.; Hudson, M. J.; Keeneb, M. T. J.; Knowlesb, J. A. *J. Mater. Chem.* **1995**, *5*, 577.
(20) Burton, A.; Accardi, R. J.; Lobo, R. F.; Falcioni, M.; Deem, M. W. *Chem. Mater.* **2000**, *12*, 2936.
(21) Gardiennet, C.; Tekely, P. *J. Phys. Chem. B* **2002**, *106*, 8928.
(22) Ai, X.; Deng, F.; Dong, J.; Chen, L.; Ye, C. *J. Phys. Chem. B* **2002**, *106*, 9237.

Table 2. Atomic Positions, Temperature Factors, Occupancies, and Multiplicities As Obtained in the Structure Refinement for RUB-39

name	*x*	*y*	*z*	*B*	occuppancy	multiplicity
Si1	0.98460(39)	0.22797(24)	0.03357(17)	1.579(46)	1.0	4
Si2	0.78322(40)	0.59974(24)	0.03940(17)	1.579(46)	1.0	4
Si3	0.07367(40)	0.42142(25)	0.17958(16)	1.579(46)	1.0	4
Si4	0.59160(39)	0.36647(24)	0.92707(16)	1.579(46)	1.0	4
Si5	0.5	0.54316(35)	0.25	1.579(46)	0.5	2
O1	0.04455(85)	0.30003(38)	0.12192(24)	2.023(92)	1.0	4
O2	0.75049(48)	0.25824(41)	0.97287(31)	2.023(92)	1.0	4
O3	0.68652(81)	0.49858(36)	0.96578(30)	2.023(92)	1.0	4
O4	0.94673(73)	0.53488(42)	0.12256(26)	2.023(92)	1.0	4
O5	0.30694(43)	0.45653(45)	0.22389(36)	2.023(92)	1.0	4
O6	0.0	0.38840(68)	0.25000	2.023(92)	0.5	2
O7	0.02479(93)	0.08275(28)	0.04910(37)	0.084(248)	1.0	4
O8	0.11446(75)	0.28946(40)	0.98887(34)	2.023(92)	1.0	4
O9	0.39223(58)	0.34366(42)	0.94025(36)	2.023(92)	1.0	4
O10	0.52708(85)	0.36771(42)	0.82786(17)	2.023(92)	1.0	4
N1	0.0	0.91785(90)	0.25(0)	22.998(999)	0.5	2
C1	0.14212(130)	0.01384(110)	0.30762(81)	17.258(490)	1.298(6)	4
C2	0.34242(129)	0.05028(152)	0.31305(61)	17.258(490)	1.298(6)	4
C3	0.49396(162)	0.10076(126)	0.39771(60)	17.258(490)	1.298(6)	4
C4	−0.07907(189)	0.83719(100)	0.30073(71)	17.258(490)	1.298(6)	4

Table 3. Selected Bond Lengths with Estimated Standard Deviation of the Silicate Layer and the Intercalate SDA

atom1−atom2	distance, Å	atom1−atom2	distance, Å
Si1−O1	1.6108(49)	Si4−O2	1.5929(53)
Si1−O2	1.6122(55)	Si4−O3	1.5944(51)
Si1−O7	1.5864(42)	Si4−O9	1.5943(60)
Si1−O8	1.6126(65)	Si4−O10	1.5908(40)
Si2−O3	1.5967(52)	Si5−O5 (×2)	1.5856(51)
Si2−O4	1.5900(52)	Si5−O10 (×2)	1.6055(44)
Si2−O8	1.5942(59)		
Si2−O9	1.5961(60)		
Si3−O1	1.6040(49)	N1−C1 (×2)	1.5006(138)
Si3−O4	1.5931(53)	N1−C4 (×2)	1.5233(138)
Si3−O5	1.5868(55)	C1−C2	1.4822(159)
Si3−O6	1.5861(34)	C2−C3	1.5158(151)

Table 4. Selected Bond Angles for the Silicate Layer and the Intercalate SDA

atom1−atom2−atom3	angle, deg	atom1−atom2−atom3	angle, deg
O1−Si1−O2	107.818(461)	O5−Si5−O5	108.270(446)
O1−Si1−O7	110.685(409)	O5−Si5−O10	109.732(479)
O1−Si1−O8	107.312(518)	O5−Si5−O10	111.098(463)
O2−Si1−O7	112.096(482)	O5−Si5−O10	111.098(463)
O2−Si1−O8	106.337(520)	O5−Si5−O10	109.732(479)
O7−Si1−O8	112.319(482)	O10−Si5−O10	106.927(349)
O3−Si2−O4	109.692(466)		
O3−Si2−O8	111.072(483)	Si1−O1−Si3	154.215(362)
O3−Si2−O9	108.664(503)	Si1−O2−Si4	144.666(393)
O4−Si2−O8	109.942(481)	Si2−O3−Si4	154.988(373)
O4−Si2−O9	108.810(515)	Si2−O4−Si3	155.763(383)
O8−Si2−O9	108.612(550)	Si3−O5−Si5	156.646(366)
O1−Si3−O4	110.063(456)	Si3−O6−Si3	154.206(339)
O1−Si3−O5	108.761(482)	Si1−O8−Si2	155.760(429)
O1−Si3−O6	108.126(383)	Si2−O9−Si4	148.444(434)
O4−Si3−O5	109.766(499)	Si4−O10−Si5	143.268(293)
O4−Si3−O6	110.768(433)		
O5−Si3−O6	109.313(366)	C1−N1−C1	93.376(1225)
O2−Si4−O3	110.141(440)	C1−N1−C4	116.929(1299)
O2−Si4−O9	109.362(488)	C1−N1−C4	116.929(1299)
O2−Si4−O10	111.246(429)	C1−N1−C4	109.035(1292)
O3−Si4−O9	109.470(518)	C4−N1−C4	110.801(1393)
O3−Si4−O10	108.981(407)	N1−C1−C2	127.140(1226)
O9−Si4−O10	107.591(501)	C1−C2−C3	116.269(1379)

polarization (CP) experiments, CP MAS NMR, with contact time of 5 ms, drastically increase the intensity of the signal at −104.4 ppm with respect to the Q^4-signals because of the preferential magnetization transfer through the attached proton, thus confirming the assignment of the signal as belonging to Q^3-silicon species. It is also interesting to note

Table 5. Distance Restraints Used in the Rietveld Refinement[a]

distance restraint (Å)	
d(Si−Si)	3.09(3)
d(Si−O)	1.595(4)
d(O−O)	2.620(9)
d(N1−C1)	1.528(9)
d(N1−C4)	1.528(9)
d(C1−C2)	1.528(9)
d(C2−C3)	1.528(9)

[a] Values for bond distances are given in Å with estimated standard deviation (ESD) in brackets. The weighting scheme used is 1/ESD.

that the Q^3-signal has increased line width as compared to the Q^4-signals. This might be due to coupling interaction with protons which was not removed completely through high power decoupling or a nonuniform environment around the Q^3-silicon atoms. The difference in local geometry of the Q^3-site with respect to the Q^4-Si also shows up in the spinning side bands for Q^3-species only, indicating that chemical shift anisotropies and/or dipolar interaction are unusually high for this layer silicate and were not averaged out through fast spinning the sample about the magic angle. With a sample spinning frequency of ∼4 kHz, these interactions were canceled for all Q^4-signals.

Thermal analysis confirms the VT ^{1}H SS MAS NMR experiments in as such that additional weight loss is only observed at rather elevated temperatures (Figure 5). For a heating rate of 5°/min a sluggish weight loss of the dehydrated sample sets in at ∼ 170 °C and accounts for approximately 1% of the total mass up until 270 °C. At ∼270 °C decomposition of the SDA leads to a drastic loss in weight (ca. 15%), and finally at 470 °C the condensation of the layers adds another approximately 2% to a total of 18% weight loss in the temperature range between RT and 600 °C. Details of the thermally induced processes will be discussed later in the article. Obviously, condensation of layers sets in locally after removal of the organic template.

Structure analysis of the dehydrated form of RUB-39 was performed to allow for the detailed analysis of the intercalated SDA and of the strong hydrogen bond. The model of the crystal structure of RUB-39 has been deduced from the zeolite framework structure of RUB-41.[5] By comparing the unit cell parameters of RUB-39 with those of RUB-41, the

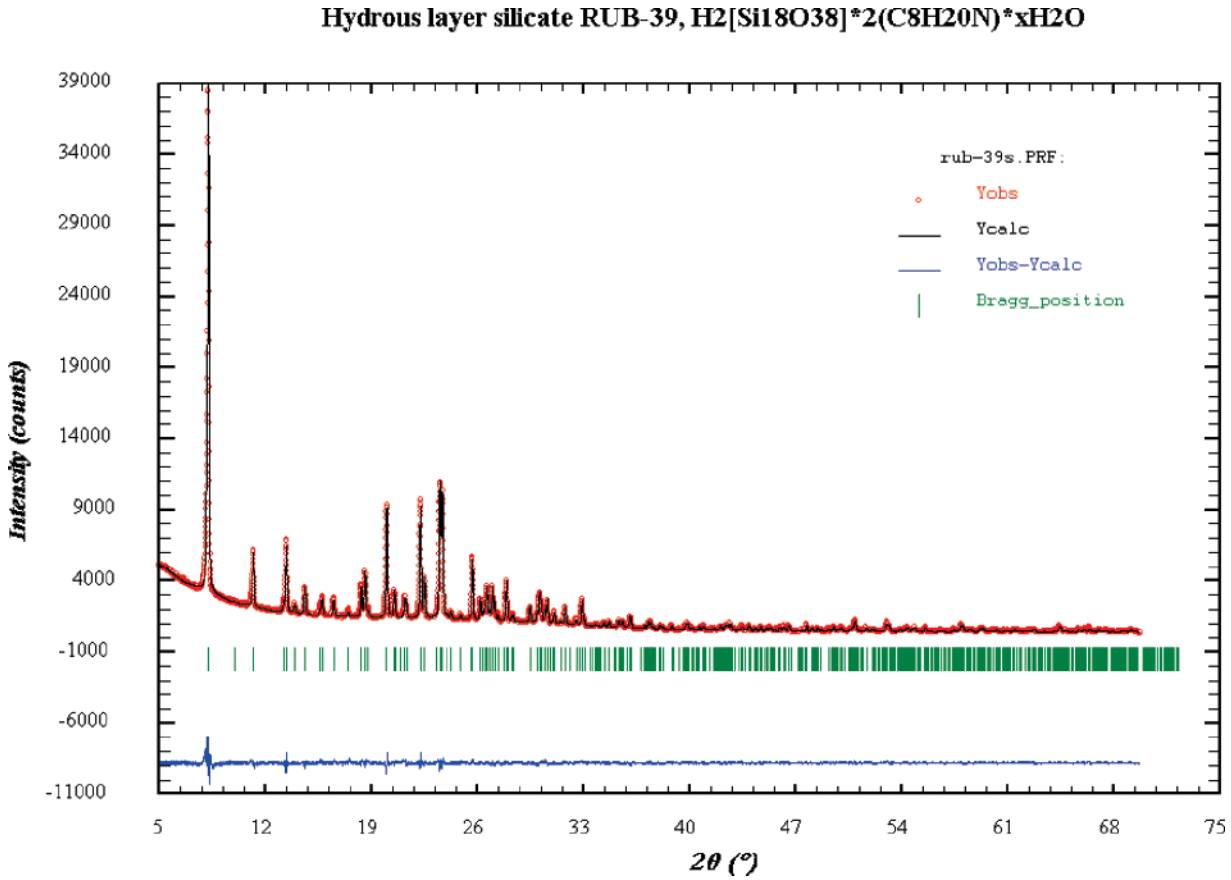

Figure 1. Results of the Rietveld structure analysis of laboratory X-ray powder diffraction data of RUB-39. Experimental and calculated data are in the upper trace, and the difference plot is shown below. Tick marks for allowed reflection are given.

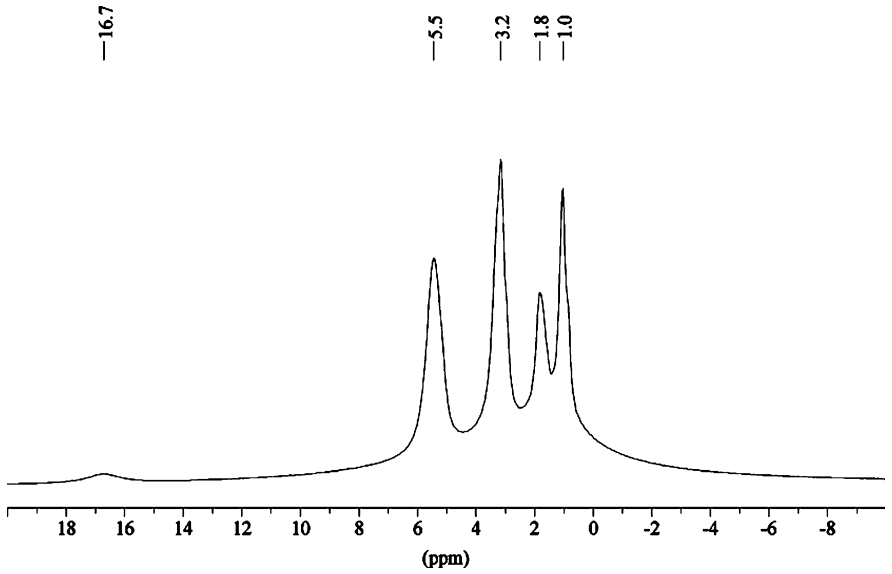

Figure 2. SS MAS ^{1}H NMR spectrum of as synthesized RUB-39 showing the three sets of proton signals. At 16.7 ppm, the strong H-bond proton shows up, at 5.5 ppm protons from hydrate water are seen, and finally, the three signals at 3.2, 1.8, and 1.0 ppm indicate the protons from the organic SDA.

shrinking along the *b* direction shows up clearly, whereas the lattice parameters for *a* and *c* remain unchanged. Therefore, we assumed that the precursor RUB-39 has the same layered building unit as its calcination product RUB-41. Because of the high number of Q^4-silicon atoms, the silicate layer is rather rigid allowing for direct import of its connectivity and geometry as obtained from the structure analysis of RUB-41. The [SiO_4]-tetrahedra form 4─4═1 secondary building units[13] connected to one-dimensional chains parallel to [201]. Neighboring chains share oxygen atoms and extend to layers which can be considered as a rigid subunits (Figure 6). The positions of 10 unique O atoms of the silicate layer and 1 N atom were obtained using the simulated annealing routine provided by the program TOPAS.[23] The structural parameters of these atoms were used

(23) *TOPAS*, software for analysis of powder diffraction data. BRUKER-AXS, http://www.bruker-axs.de.

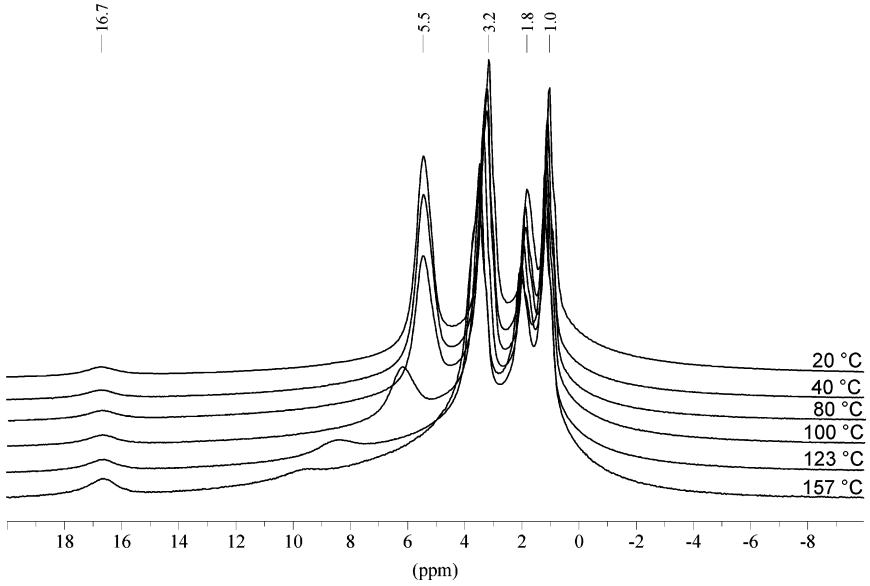

Figure 3. VT MAS ^{1}H NMR spectra in the temperature range between RT and 157 °C. The dehydration of the layer silicate causes no structural changes in RUB-39 detectable with ^{1}H NMR.

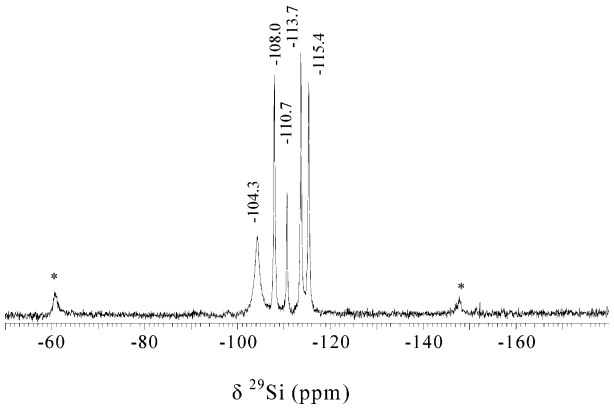

Figure 4. ^{29}Si MAS NMR spectrum of as-synthesized RUB-39. The broadened low field signal at −104.3 ppm indicates the presence of Q^3-Si entities, and the four sharp signals at higher field are assigned to Q^4-Si of the layer. It is worth noting that the spinning side band results only from Q^3-Si due to its increased chemical shift anisotropy.

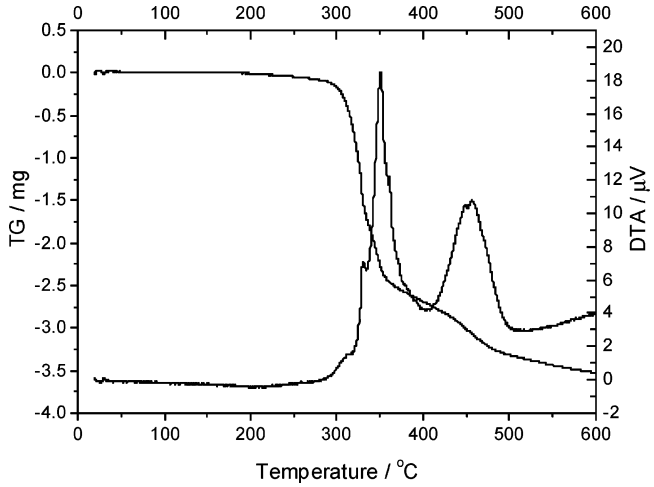

Figure 5. Thermal analysis of dehydrated RUB-39 showed in the thermogravimetric curve weight loss starting at ∼290 °C due to the thermal degradation of the SDA. In a second step, further weight loss is realized because of the condensation of the silicate layers and the corresponding weight loss. The continuous slope of the thermogravimetric curve indicates sluggish progress of the reaction.

subsequently in Rietveld refinement with the program FULLPROF.[12] The remaining C atoms were located from Fourier syntheses. On the basis of chemically reasonable geometries, soft distance restraints for d_{Si-Si}, d_{Si-O}, d_{O-O}, d_{N-C}, and d_{C-C} (Table 5) were set on during the refinement. The parameters used for the refinement are summarized in Table 1. The structure parameters of RUB-39 are listed in Table 2. Selected bond lengths and bond angles are shown in Tables 3 and 4, respectively.

In Figure 6 the *x*,*z*-projection of the structure is shown representing the silicate layer as skeleton model connecting the Si atom in the centers of the [SiO_4]-tetrahedra with each other. The cage-like subunit is color coded as a guide for the eye. For clarity the oxygen atoms are not shown and should be near the middle between the tetrahedral nodes. The SDA, dimethyldipropylammonium cation, is shown as a skeleton model with the positions of the C- and N-atoms, however without hydrogens. Figure 7 shows a *y*,*z*-projection of the structure with the strong hydrogen bond connecting neighboring layers indicated in blue. Only the oxygen atoms carrying the hydrogen connecting the silicate layers via

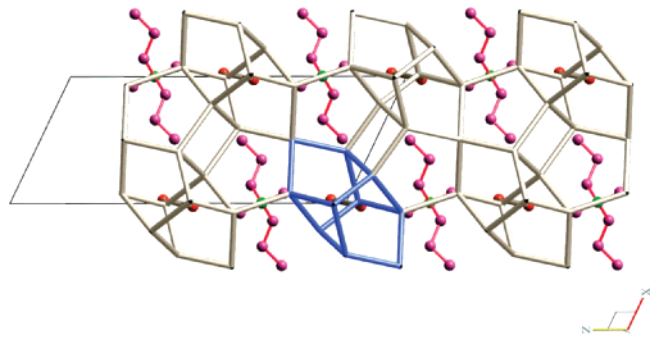

Figure 6. Projection of the structure of RUB-39 parallel to [010] showing the skeleton of the silicate layer (only centers of [$SiO]_4$ tetrahedra are shown] and the tetraalkylammonium cation as a ball-and-stick molecule without hydrogen. The projection of the silicate skeleton resembles the [010] projection of zeolite HEU.

hydrogen bonds are included. In Figure 8 the *y*,*z*-projection of the structure is shown as a ball-and-stick model including the framework oxygens and highlighting the hydrogen bond

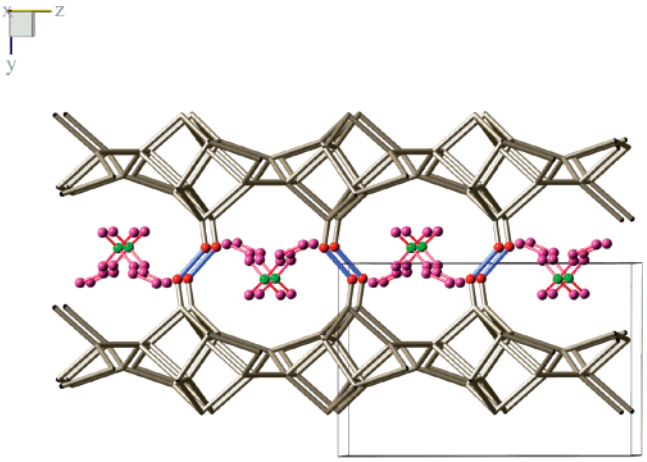

Figure 7. Projection of the crystal structure of RUB-39 on the *y*,*z* plane. The silicate layer is represented by a skeleton model with the silicon in tetrahedral centers. The organic tetraalkylammonium cation is shown as a ball-and-stick molecule without hydrogens.

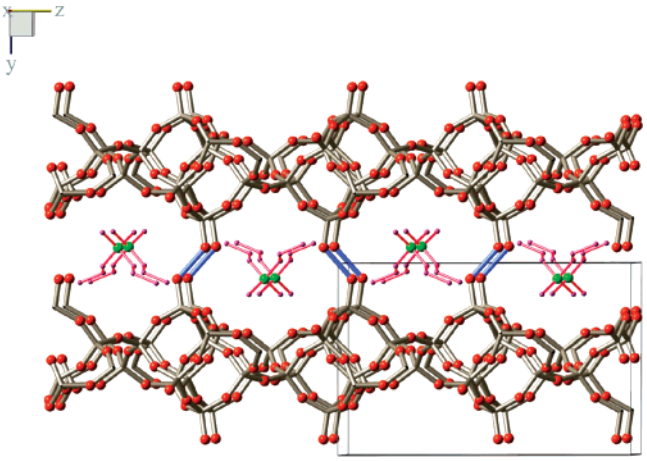

Figure 8. Projection of the crystal structure of RUB-39 on the *y*,*z* plane. The silicate layer is represented by a ball-and-stick derived model with the silicon in the tetrahedral center. The organic tetraalkylammonium cation is shown as a ball-and-stick molecule without hydrogens.

connecting neighboring layers with $d(O-O) = 2.388$ Å in agreement with the downfield shifted ^{1}H NMR signal at approximately 16.8 ppm. This very short and strong hydrogen bond is of particular importance for the periodic order of the silicate layers in the crystal and, at the same time, provides for the stability for the pore housing the organic SDA. In the as-synthesized state the pore opening between neighboring layers corresponds almost to 10 × 12 MR channel systems of three-dimensional frameworks of silicate zeolites leaving enough space for the incorporation of the SDA molecules. The hydrogen bridge−pillar connecting two layer-terminating siloxy groups leave a net charge of −1 per hydrogen bridge which is compensated by the SDA cation leading to an electroneutral composite.

From the structure analysis of the hydrate water free form of RUB-39 one can only speculate about the location of the additional hydrate water molecules which were set free in the preparation of the material for structure analysis. As can be seen from the ^{1}H VT MAS NMR spectra below 70 °C (Figure 3), the proton signal at 5.5 ppm is typical for the free water molecules and shifts slightly to lower field upon further heating. At the same time, the signal becomes broader. At 123 °C the chemical shift of the proton signal is at 8.4 ppm, further shifting to almost 10 ppm at 157 °C. The significant low-field shift signifies either increasing acidity, which is very unlikely, or involvement in hydrogen bonding through exchange processes, thus interacting with the strong hydrogen bond connecting the silicate layers. After heating the sample at 160 °C for 4 days the signal for the water protons has disappeared completely and at the same time the line width of the signals from protons of the hydrocarbon chains of the SDA have considerably broadened. This leads to severe overlap of the formerly three resolved signals indicating structural rearrangement and strong coupling interaction (Figure 9). The NMR results of the dehydrated material are somewhat in contrast to the clear picture of the location and structure of the SDA from Rietveld analysis. Here, the organic SDA is geometrically well-defined in a highly extended configuration. However, NMR is a local probe very sensitive to small local variations in structure, statically or dynamically, added up in the spectrum, whereas diffraction experiments present results averaging structural features in time and space; thus, the findings are not contradictory but complement each other.

The strong hydrogen bond is almost unaffected from the dehydration process as indicated by the proton signal remaining at ∼16.7 ppm. The spectra taken after thermal treatment at 123 and 157 °C, however, show a slight shift of the signal to 16.9 ppm indicating weak exchange interaction (Figure 3). This is concurrent with the low-field shift of the water proton signal, thus confirming the interaction. On the basis of these observations it is concluded that the hydrate water molecules reside in the interlayer space in proximity to the hydrogen bridge and in contact with the methyl-substituted side of the SDA (cf. Figures 6−8).

To summarize, the structure refinement together with the results of SS NMR experiments of the new hydrated layer silicate RUB-39 yield a very consistent picture of the crystal structure including bond lengths and angles which are in ranges expected from crystal chemistry considerations.

Hydrogen Bonding and SDA Cations between Layers. As observed for most layer silicates, RUB-39 crystallizes with platy morphology indicating that the formation of strong silicate bonds is fast and the formation of a new silicate layer along [010] is the rate determining process. The surface termination most likely is the SDA saturated silicate layer with hydrogen bridges to the solvent water. The SDA fills the void space created by the corrugated surface of the silicate layer, whereas the silanol group anchors silicate species as starting seeds for the formation of new layers. The fact that the interlayer hydrogen bridge is so strong leads to the high degree of stacking order which is unusual for hydrous layer silicates. In addition to ^{1}H SS NMR experiments and results from Rietveld structure refinement, Fourier transform infrared (FTIR) data (Figure 10) also confirm the very strong hydrogen bridge with a broad intensity of the O−H-stretching frequency in the range between 3500 and 2500 cm^{-1}. The spectrum of the dehydrated sample also confirms that no free water is left inside the structure. The weak and sharp peaks in this range are due to C−H modes of the SDA.

Structure analysis of a number of hydrous layer silicates with Na or alkylammonium cations (e.g., refs 3, 16, 18, 20,

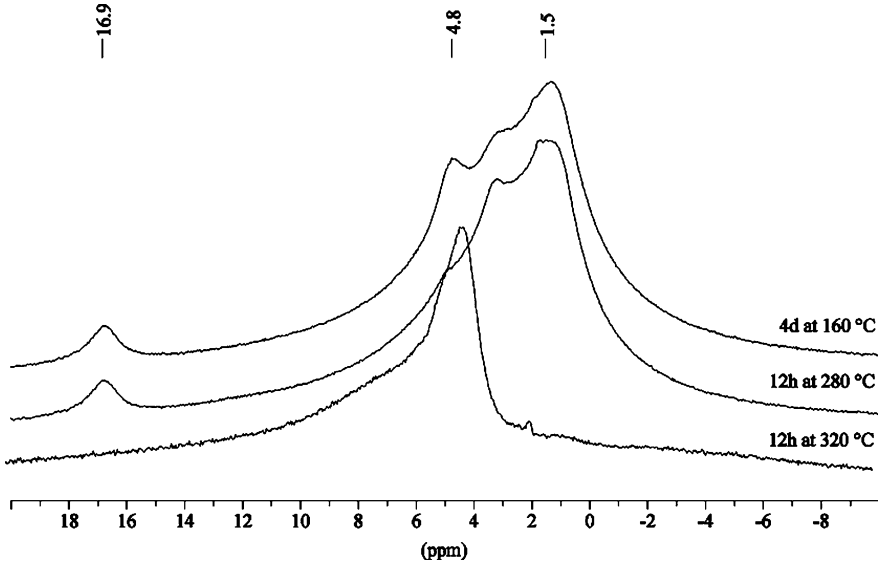

Figure 9. VT ^{1}H MAS NMR spectra showing the condensation reaction in snapshots. As long as the low-field proton signal typical for the interlayer hydrogen bond shows up, the SDA is present as documented by the proton signal in the range between 4.8 and 1.5 ppm, and layered structure of RUB-39 is maintained. No "empty" RUB-39 has been observed. Degradation of the SDA leads to condensation of layers yielding zeolite RUB-41 as shown in the ^{1}H MAS NMR spectrum taken after annealing RUB-39 for 12 h at 320 °C. The low field signal has disappeared, wheareas the much reduced signal at 4.8 ppm indicates residual protons from SDA degradation.

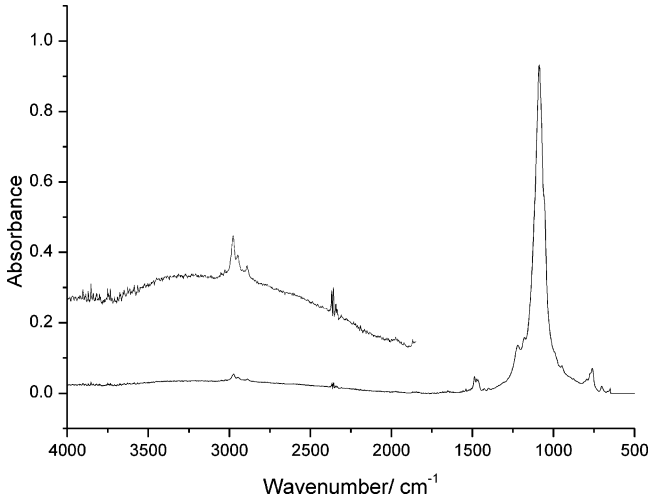

Figure 10. FTIR spectrum of RUB-39. The broad absorption between 3500 and 2500 cm^{-1} indicates the strong hydrogen bridge (see enlarged insert).

and 24) as charge compensating entities all show low field shifted proton NMR signals indicating strong hydrogen bonds. However, most other systems studied so far have intra-layer hydrogen bonds connecting neighboring siloxys. In these cases interlayer periodic coherence is established with much weaker bonding interaction involving intercalated water layers hydrating the charge compensating cations. The rather weak and non-directional Coulomb bond leads to considerable stacking disorder in the respective crystal structure and, consequently, to problems in structure solution and refinement. This might be the reason why the crystal structures of hydrous layer silicates such as Magadiite and Kenyaiite still are unknown, although the minerals have been known for more than 50 years.

Condensation Process of RUB-39 to RUB-41. As resulted from thermogravimetry (Figure 5), the total weight loss of the sample in the temperature range from RT to 600 °C in air is about 18−19% due to the decomposition, combustion, and removal of the organic SDA and the subsequent condensation of neighboring silicate layers. The fact that there is no weight loss below 250 °C indicates that there is no further hydrate water intercalated in the structure of the gently dried sample of RUB-39. The first exothermic maximum at 350 °C is accompanied with a 13% weight loss indicating the breakdown and removal of the SDA followed by a second thermal signal centered at 460 °C for the condensation reaction. Most likely, the signals in thermal analysis are a superposition of various processes of exothermic and endothermic nature, such as SDA decomposition (endo) and combustions (exo), coinciding with the condensation of silicate layers (endo). Because the combustion reaction dominates, only exothermic maxima are observed. It is proposed that the condensation process from RUB-39 to RUB-41 during the calcinations is described by the following equation:

$$\underset{\text{RUB-39}}{H_2[Si_{18}O_{38}]\cdot 2(C_8H_{20}N)} \xrightarrow[\Delta]{\text{air}} \underset{\text{RUB-41}}{18SiO_2} + 11H_2O + NO_x + yCO + zCO_2$$

No matter how complex the decomposition process is and which gaseous products are formed, we can estimate the percentage of the weight loss according to the above equation. The calcination of RUB-39, which leads to the SiO_2-polymorph RUB-41, is quantitative. The mass ratio of RUB-41/RUB-39 is 78.6%, so the theoretically calculated weight loss should be 21.4%. The results of elemental analysis are shown in Table 6. The sum of the content of C, N, H, and O (the theoretical data were taken) is 19.6%, somewhat lower than theoretically expected, but is consistent with the data of thermal analysis. The difference might be due to non-stoichiometric occupation of SDA cations inside

(24) Vortmann, S.; Rius, J.; Marler, B.; Gies, H. *Eur. J. Mineral.* **1999**, *11*, 125.

Table 6. Element Analysis of As-Made RUB-39

	C	N	H	O
experimental wt %	12.77	1.72	2.85	n.d.
theoretical wt %	14.0	2.0	3.1	2.3

RUB-39 and on the atmospheric gases adsorbed inside the channels of RUB-41 after calcination.

From the DTA analysis it seems likely to decompose the SDA of RUB-39 without condensation of the silicate layer. In the temperature range between 350 and 400 °C the organic SDA seemingly has been removed from RUB-39; however, the condensation of layers has not started yet. At the same time, the sluggish condensation process seems to offer the opportunity to study the details of the mechanism of the reaction. VT XRD of the calcination/condensation process shows line broadening and vanishing intensities of RUB-39 and the appearance of RUB-41 in the transition temperature. Therefore, attempts were made to selectively calcine samples at fixed temperature so that only SDA is removed. For this purpose, samples were heated overnight at temperatures ranging from 280 to 350 °C in steps of 10°. For each temperature RT NMR spectra were recorded. ^{13}C and ^{29}Si SS NMR experiments revealed that as long as there is a carbon signal, the ^{29}Si spectrum of RUB-39 is observed and the signal is for RUB-39 only. After calcination at 320 °C all of sample had been converted to RUB-41 without stabilizing the reaction intermediate. The process is also nicely reflected in ^{1}H NMR spectra. As long as there is a strong signal for protons from the SDA the low field proton is present. After collapse of the SDA (320 °C tempering) a weak proton signal at ~4.8 ppm was observed; however, the low field signal for the hydrogen bridge bonded proton is no longer present. The residual proton signal is likely to be due to structural defects from dangling Si−OH groups. Obviously, the SDA acts as spacer stabilizing the open arrangement of silicate layers. As soon as it is removed, the silanol groups condense to form proper Si−O−Si bridges, setting H_2O free. In general, the formation of only two Si−O−Si bridges between neighboring layers already freezes their position leading to a well-organized condensation process which finally yields a highly crystalline three-dimensional SiO_2 framework.

Conclusions

Crystal structure analysis of the new hydrous layer silicate RUB-39 shows that very short hydrogen bonds between neighboring layers are responsible for the perfect, topotactic condensation of silicate layers yielding a well-ordered calcination product, zeolite RUB-41. The ^{1}H SS NMR spectra confirm the findings of the Rietveld structure refinement. RUB-39 is one of few hydrous layer silicates with strong interlayer hydrogen bonds which have been analyzed with diffraction experiments. The results show that in this way new framework silicates can be obtained through topotactic condensation of the layer silicate leading to new materials with structural characteristics due to specific synthesis conditions of the layered precursor. The importance of structural studies is demonstrated, enabling mechanistic understanding of the transformation process and thoughtful planning of further experiments.

As a follow-up project the insertion of Al, B, and other functional T-atoms into the layered precursor as well as its condensation to three-dimensional framework silicate zeolites has been achieved and will be reported in the near future.

Acknowledgment. Financial assistance from DFG, Project No. Gi-139/24, is acknowledged; BASF supported our research through generous donations of chemicals.

CM0706907